Synchrotron Mössbauer source of ^{57}Fe radiation

G.V. Smirnov

Russian Research Center "Kurchatov Institute", 123182 Moscow, Russia

A non-radioactive source of Mössbauer radiation is described for use in Mössbauer absorption and scattering spectroscopy. The radiation is generated by synchrotron X-rays in an iron borate single crystal set in diffraction conditions at the Néel temperature (75.3°C). Like a conventional Mössbauer source the new Synchrotron Mössbauer (SM) source emits single-line radiation of about natural linewidth, but in addition the emitted radiation is fully recoilless, highly directed and of pure linear polarization. An extremely high suppression of the electronic scattering is achieved. The latter circumstance allows one to perform Mössbauer experiments using pulsed synchrotron radiation in a steady state mode as in a normal Mössbauer measurement.

The theory of the SM source is developed. First Mössbauer spectra obtained with the SM source are shown. Applications of the SM source are discussed.

1. Introduction

Stan Ruby was the first who suggested to use synchrotron radiation (SR) in Mössbauer spectroscopy [1].[1] In his scheme all components of a Mössbauer transition are excited by a broad band X-ray SR. The delayed radiation transmitted through the sample is analyzed in the energy domain with a resonant detector by Doppler shifting the sample resonances with respect to those of the analyzer. Such an analysis reveals a reduction of the transmitted radiation at the resonance energies, thus yielding the Mössbauer spectrum of the sample. The accomplishment of such a kind of measurement faces, however, a great difficulty because of a huge non-resonant background practically inescapable in this experiment.

A different technique was developed to study the nuclear γ-resonance with the use of SR. The pulsed radiation emitted by electrons orbiting in a storage ring provides perfect conditions for time-resolved measurements of nuclear resonance scattering [2,3]. The parameters of the resonance shape and its hyperfine structure can be retrieved from the time dependence of the delayed coherent emission of nuclei excited by SR pulses. The unique properties of SR and the measurement technique suggest various interesting applications. The time domain technique, in particular, has been developing rapidly, providing an efficient way to study the nuclear γ-resonance (for recent reviews see, e.g., [4,5]).

[1] For a historical introduction to synchrotron radiation Mössbauer spectroscopy also see chapter I of this issue.

Nevertheless, the original idea to use SR in order to perform a measurement of nuclear resonant absorption or scattering in the energy domain remains very attractive because the high directionality, the degree of polarization and other properties of SR offer quite new possibilities for performing Mössbauer experiments. Moreover, the time and energy domain measurements combined at one and the same SR facility can provide valuable complementary information.

To produce Mössbauer radiation with the help of SR it was suggested to use electronically forbidden but nuclear allowed Bragg reflections, so called pure nuclear reflections. They can be obtained by employing the polarization dependence of the nuclear resonance susceptibility. Those crystals where internal magnetic field or electric field gradient spatial distributions do not show the same symmetry as the electron charge should exhibit additional reflections related to 3-dimensional structures of the magnetic or electric field. The polarization dependence of the nuclear susceptibility is intrinsically related to the hyperfine interaction. Therefore, the presence of hyperfine interaction is a necessary condition for obtaining a pure nuclear reflection. This is why pure nuclear Bragg reflections usually have a multiline resonance structure, see, e.g., [6]. However, a particular case of a pure nuclear reflection was found in [6], which is well matched to the idea of extraction of a single-line nuclear component of SR. Pure nuclear reflectivity within an energy band of about the natural width of the nuclear level was obtained when an $^{57}FeBO_3$ (iron borate) single crystal was heated in an external magnetic field to the Néel temperature T_N. The first studies of the time dependence of the pure nuclear reflection of SR in the vicinity of T_N were reported in [7].

In the following section we describe the theory of pure nuclear diffraction in iron borate where sublevels of the excited state of the ^{57}Fe nucleus turned out to be mixtures of $|m\rangle$-states due to combined magnetic dipole and electric quadrupole interaction. The experimental studies of the diffraction with convential Mössbauer radiation and SR are discribed in section 3. The parameters of the synchrotron Mössbauer (SM) source are presented and the first Mössbauer spectra taken with the SM source are shown. Some prospects of the application of synchrotron Mössbauer sources are discussed in section 4.

2. Theory of pure nuclear diffraction in $^{57}FeBO_3$

To solve the problem of scattering from a nuclear ensemble one has first of all to find the nuclear susceptibility (see section 2.2). In an optically active medium where the polarization state of radiation is changed by coherent scattering and in the case of several allowed directions for coherent scattering the susceptibility splits into several elements presenting the relative transition probabilities between the polarization states and directions. The full set of the susceptibility elements can be organized in matrix form. To find the nuclear susceptibility matrix one first describes the nuclear states involved in the excited transition and then performs the summation of all scattering paths from the crystal unit cell taking into account all particular nuclear transitions (between the ground and the first excited states of ^{57}Fe in our case). When the nuclear

susceptibility matrix is defined one solves Maxwell's dynamical equations taking into account the boundary conditions to get the desired reflectivity. We accomplish this plan step by step in the following subsections.

2.1. *^{57}Fe nuclear states in the crystalline field of $^{57}FeBO_3$*

As is well known, the ^{57}Fe nucleus in the first excited state possesses both a magnetic and a quadrupole moment, while in the ground state it has only a magnetic moment. An iron nucleus in $^{57}FeBO_3$ is under the influence of the crystalline field, which is a combination of a uniform magnetic field and an electric field gradient of axial symmetry. So, the nucleus experiences a magnetic dipole interaction in the ground state and a combined magnetic dipole and axially symmetric electric quadrupole interaction in the excited state. The splitting of nuclear states in similar conditions has been treated by several authors, see e.g. [8–13]. The theory and calculations described here are for a nuclear M1 transition with $I_{\rm g} = \frac{1}{2},\ I_{\rm e} = \frac{3}{2}$ the spins of the ground and the excited nuclear states, respectively.

The Hamiltonian of the magnetic dipole interaction in the ground state looks quite simple in the coordinate system where the magnetic field B lies along the z axis chosen as an axis of quantization:

$$\widehat{H}_{\rm g} = -g_{\rm g}\mu_{\rm n}B\hat{I}_z, \tag{2.1}$$

where $g_{\rm g}$ is the nuclear g-factor in the ground state, $\mu_{\rm n}$ is the nuclear magneton and $\hat{I}_z$ is the operator of the z-component of the nuclear spin. The eigenvalues and the eigenfunctions of this Hamiltonian are easily found:

$$E_1^{\rm g} = -\tfrac{1}{2}g_{\rm g}\mu_{\rm n}B\colon\ |\Phi_1\rangle = \big|+\tfrac{1}{2}\big\rangle, \qquad E_2^{\rm g} = +\tfrac{1}{2}g_{\rm g}\mu_{\rm n}B\colon\ |\Phi_2\rangle = \big|-\tfrac{1}{2}\big\rangle. \tag{2.2}$$

The eigenfunctions $|\Phi\rangle = |m_{\rm g}\rangle$ present the dependence only on the spin projection variable. Since $g_{\rm g} > 0,\ E_1^{\rm g} < E_2^{\rm g}$.

The Hamiltonian $\widehat{H}_{\rm e}$ of the combined hyperfine interaction in the excited state can be thought of as sum of two parts, presenting the magnetic dipole and the electric quadrupole interaction energy. We chose the z direction as direction of the magnetic field. The electric field gradient in a $^{57}FeBO_3$ crystal is perpendicular to the magnetic field. We direct it along the x axis. In the temperature region close to the magnetic phase transition, the quadrupole interaction becomes dominant and the error due to the canting angle between the magnetic sublattices in the crystal can be disregarded. For the quantization axis along the magnetic field the Hamiltonian of the combined interaction can be shown to be

$$\widehat{H}_{\rm e} = -\omega_B\hbar\hat{I}_z - \tfrac{1}{2}\omega_E\hbar\big\{3\big[\hat{I}_z^2 + \tfrac{1}{2}\big(\hat{I}_+^2 - \hat{I}_-^2\big)\big] - I(I+1)\big\}, \tag{2.3}$$

where

$$\omega_B = \frac{g_{\rm e}\mu_{\rm n}B}{\hbar} \quad \text{and} \quad \omega_E = \frac{1}{2}\frac{eQ}{\hbar}\frac{\partial^2 V_{\rm el}}{\partial x^2}\frac{1}{2I(2I-1)},$$

$g_{\rm e}$ is the nuclear g-factor in the excited state, e – the charge of the proton, Q – the nuclear electric quadrupole moment, $V_{\rm el}$ – the electric field potential. The operators $\hat{I}_{\pm} = \hat{I}_x \pm \hat{I}_y$ are the step-up and step-down spin operators raising and lowering the spin projection by $\Delta m = \pm 1$ [15]:

$$\hat{I}_{\pm}|I, m\rangle = \Gamma_{\pm}|I, m \pm 1\rangle, \tag{2.4}$$

where $\Gamma_{\pm} = \sqrt{(I \mp m)(I \pm m + 1)}$. Applying eq. (2.4) for the spin $I_{\rm e} = \frac{3}{2}$ we obtain

$$\tfrac{1}{2}\big(\hat{I}_+^2 - \hat{I}_-^2\big)|m_{\rm e}\rangle = \begin{cases} \sqrt{3}|m_{\rm e} - 2\rangle & \text{for } m_{\rm e} = +\frac{3}{2}, +\frac{1}{2}, \\ \sqrt{3}|m_{\rm e} + 2\rangle & \text{for } m_{\rm e} = -\frac{1}{2}, -\frac{3}{2}. \end{cases} \tag{2.5}$$

Here the operator at the left-hand side is the part of the Hamiltonian equation (2.3) and $|m_{\rm e}\rangle$ are eigenfunctions of pure states in spin projection of the excited nuclear state. An eigenfunction of the total operator $\widehat{H}_{\rm e}$ can be expressed as a linear combination of the eigenfunctions corresponding to the pure magnetic interaction, $|m_{\rm e}\rangle$, which form a complete set

$$\Lambda_j = c_j^{-3/2}\big|-\tfrac{3}{2}\big\rangle + c_j^{-1/2}\big|-\tfrac{1}{2}\big\rangle + c_j^{+1/2}\big|+\tfrac{1}{2}\big\rangle + c_j^{+3/2}\big|+\tfrac{3}{2}\big\rangle, \tag{2.6}$$

where c_j^m are the probability amplitudes of the relevant spin projections in the excited jth state. The eigenfunction Λ_j of $\widehat{H}_{\rm e}$ satisfies the equation

$$\widehat{H}_{\rm e}\Lambda_j = E_j^{\rm e}\Lambda_j, \tag{2.7}$$

where $E_j^{\rm e}$ are eigenvalues of the total Hamiltonian. We substitute $\widehat{H}_{\rm e}$ in the explicit form (eq. (2.3)), in eq. (2.7), divide the equation by $\omega_E\hbar$ and with eq. (2.5) obtain

$$\begin{aligned} &c_j^{-3/2}\big[3(\nu-1)\big|-\tfrac{3}{2}\big\rangle + 3\sqrt{3}\big|+\tfrac{1}{2}\big\rangle\big] + c_j^{-1/2}\big[(\nu+3)\big|-\tfrac{1}{2}\big\rangle + 3\sqrt{3}\big|+\tfrac{3}{2}\big\rangle\big] \\ &\quad + c_j^{+1/2}\big[-(\nu-3)\big|+\tfrac{1}{2}\big\rangle + 3\sqrt{3}\big|-\tfrac{3}{2}\big\rangle\big] \\ &\quad + c_j^{+3/2}\big[-3(\nu+1)\big|+\tfrac{3}{2}\big\rangle + 3\sqrt{3}\big|-\tfrac{1}{2}\big\rangle\big] \\ &= 2\varepsilon_j\big[c_j^{-3/2}\big|-\tfrac{3}{2}\big\rangle + c_j^{-1/2}\big|-\tfrac{1}{2}\big\rangle + c_j^{+1/2}\big|+\tfrac{1}{2}\big\rangle + c_j^{+3/2}\big|+\tfrac{3}{2}\big\rangle\big], \end{aligned} \tag{2.8}$$

where $\nu = \omega_B/\omega_E$ and $\varepsilon_j = E_j^{\rm e}/\omega_E\hbar$. Equation (2.8) can be transformed into four scalar equations by first multiplying from the left by $\langle-\frac{3}{2}|$ and integrating over coordinates, and then repeating the procedure using $\langle-\frac{1}{2}|, \langle+\frac{1}{2}|, \langle+\frac{3}{2}|$ instead. The properties of $|m_e\rangle$ to be orthogonal to one another and normalized to unity are used. The resulting set of four equations for c_j^m is split into the two following sets of two equations:

$$\begin{aligned} -c_j^{+1/2}\big[(\nu-3) + 2\varepsilon_j\big] + c_j^{-3/2}3\sqrt{3} = 0, \\ c_j^{+1/2}3\sqrt{3} + c_j^{-3/2}\big[3(\nu-1) - 2\varepsilon_j\big] = 0 \end{aligned} \tag{2.9}$$

and

$$\begin{aligned} -c_j^{+3/2}\big[3(\nu+1)+2\varepsilon_j\big]+c_j^{-1/2}3\sqrt{3}=0,\\ c_j^{+3/2}3\sqrt{3}+c_j^{-1/2}\big[(\nu+3)-2\varepsilon_j\big]=0. \end{aligned} \tag{2.10}$$

For the nontrivial solution for the amplitudes c_j^m, the determinants of the sets of equations (2.9) and (2.10) must be zero. This condition gives rise to the following secular equations for the eigenvalues ε:

$$\big[(\nu-3)+2\varepsilon\big]\big[3(\nu-1)-2\varepsilon\big]+27=0, \tag{2.11}$$

$$\big[3(\nu+1)+2\varepsilon\big]\big[(\nu+3)-2\varepsilon\big]+27=0. \tag{2.12}$$

Both equations are quadratic in ε and each therefore has two solutions. They represent four normalized energy values of the excited state:

$$\varepsilon_{1,3}=\tfrac{1}{2}\nu\pm\sqrt{\nu^2-3\nu+9},\qquad \varepsilon_{2,4}=-\tfrac{1}{2}\nu\pm\sqrt{\nu^2+3\nu+9}. \tag{2.13}$$

Since in the excited state of ^{57}Fe the g-factor is negative, $E_1^{\mathrm{e}}\leqslant E_2^{\mathrm{e}}\leqslant E_3^{\mathrm{e}}\leqslant E_4^{\mathrm{e}}$. The eigenvalues given by eq. (2.13) are appropriate for the following four eigenfunctions (in accordance with eqs. (2.9)–(2.12)):

$$\begin{aligned} &\Lambda_1=c_1^{+1/2}\big|+\tfrac{1}{2}\big\rangle+c_1^{-3/2}\big|-\tfrac{3}{2}\big\rangle,\qquad \Lambda_2=c_2^{+3/2}\big|+\tfrac{3}{2}\big\rangle+c_2^{-1/2}\big|-\tfrac{1}{2}\big\rangle,\\ &\Lambda_3=c_3^{+1/2}\big|+\tfrac{1}{2}\big\rangle+c_3^{-3/2}\big|-\tfrac{3}{2}\big\rangle,\qquad \Lambda_4=c_4^{+3/2}\big|+\tfrac{3}{2}\big\rangle+c_4^{-1/2}\big|-\tfrac{1}{2}\big\rangle, \end{aligned} \tag{2.14}$$

i.e., the excited nuclear states are mixed over the spin projection states. The two spin projections are mixed at each nuclear substate. We use the solutions for the eigenstates, eq. (2.13), to find the amplitudes $c_j^{m_{\mathrm{e}}}$. According to eq. (2.14) the levels $\varepsilon_{1,3}$ are mixtures of the $|+\frac{1}{2}\rangle$ and $|-\frac{3}{2}\rangle$ states, and the levels $\varepsilon_{2,4}$ of the $|+\frac{3}{2}\rangle$ and $|-\frac{1}{2}\rangle$ states. For finding the amplitudes $c_1^{+1/2}$ and $c_1^{-3/2}$ we substitute ε_1 into eq. (2.9) and use the condition of normalization of Λ_1:

$$-c_1^{+1/2}B_1+c_1^{-3/2}3\sqrt{3}=0, \tag{2.15}$$

$$c_1^{+1/2}3\sqrt{3}+c_1^{-3/2}A_1=0, \tag{2.16}$$

$$\big|c_1^{+1/2}\big|^2+\big|c_1^{-3/2}\big|^2=1, \tag{2.17}$$

where we used new variables $A_1=3(\nu-1)-\varepsilon_1$ and $B_1=(\nu-3)+\varepsilon_1$. The complex amplitudes can be written in the form

$$c_1^{+1/2}=\big|c_1^{+1/2}\big|\mathrm{e}^{\mathrm{i}\varphi}\quad\text{and}\quad c_1^{-3/2}=\big|c_1^{-3/2}\big|, \tag{2.18}$$

where φ is the relative phase between the amplitudes. Substituting eq. (2.18) into eq. (2.15) and equalizing the real and imaginary parts of the expression at the left-hand side to zero yields

$$\begin{aligned} -\left|c_1^{+1/2}\right|B_1 + \left|c_1^{-3/2}\right|3\sqrt{3} = 0, \\ \varphi = 0. \end{aligned} \tag{2.19}$$

With the use of eqs. (2.19) and (2.17), after a simple transformation we obtain

$$\left|c_1^{+1/2}\right|^2 B_1^2 = 27\left(1 - \left|c_1^{+1/2}\right|^2\right),$$

the solution of which is

$$\left|c_1^{+1/2}\right| = \left(\frac{B_1^2}{27} + 1\right)^{-1/2}.$$

The same operations applied to eq. (2.16) yield the amplitude of the second spin state

$$\left|c_1^{-3/2}\right| = \left(\frac{A_1^2}{27} + 1\right)^{-1/2}.$$

Substituting ε_3 into eq. (2.9) and $\varepsilon_{2,4}$ into eq. (2.10) and repeating similar operations leads to the solutions for the amplitudes of the spin states appropriate for all the other energy sublevels in the excited nuclear state. We write down the final result:

$$\begin{aligned}
\varepsilon_1\text{:}\quad & \left|c_1^{-3/2}\right| = \left(\frac{A_1^2}{27} + 1\right)^{-1/2}, \quad A_1 = 3(\nu - 1) - 2\varepsilon_1, \\
& \left|c_1^{+1/2}\right| = \left(\frac{B_1^2}{27} + 1\right)^{-1/2}, \quad B_1 = (\nu - 3) + 2\varepsilon_1, \\
\varepsilon_2\text{:}\quad & \left|c_2^{-1/2}\right| = \left(\frac{A_2^2}{27} + 1\right)^{-1/2}, \quad A_2 = (\nu + 3) - 2\varepsilon_2, \\
& \left|c_2^{+3/2}\right| = \left(\frac{B_2^2}{27} + 1\right)^{-1/2}, \quad B_2 = 3(\nu + 1) + 2\varepsilon_2, \\
\varepsilon_{3:}\text{:}\quad & \left|c_3^{+1/2}\right| = \left(\frac{B_3^2}{27} + 1\right)^{-1/2}, \quad B_3 = (\nu - 3) + 2\varepsilon_3, \\
& \left|c_3^{-3/2}\right| = \left(\frac{A_3^2}{27} + 1\right)^{-1/2}, \quad A_3 = 3(\nu - 1) - 2\varepsilon_3, \\
\varepsilon_4\text{:}\quad & \left|c_4^{+3/2}\right| = \left(\frac{B_4^2}{27} + 1\right)^{-1/2}, \quad B_4 = 3(\nu + 1) + 2\varepsilon_4, \\
& \left|c_4^{-1/2}\right| = \left(\frac{A_4^2}{27} + 1\right)^{-1/2}, \quad A_4 = (\nu + 3) - 2\varepsilon_4.
\end{aligned} \tag{2.20}$$

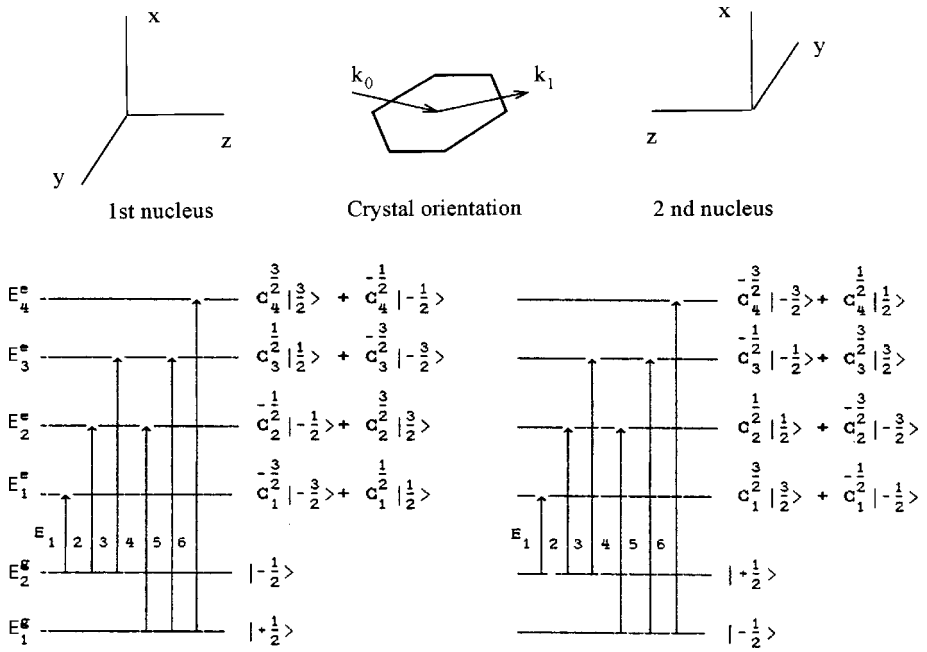

Figure 1. Scheme of energy levels in the ground and excited states of ^{57}Fe nuclei in the unit cell of antiferromagnetic $FeBO_3$. The coordinate axes at the nuclei are chosen so that the magnetic hyperfine field is directed along the z axis, while the main axis of the electric field gradient lies along the x axis. Under these conditions the nuclear excited states are sums over spin projection eigenstates $|m\rangle$ as shown in the figure. The scattering geometry is displayed schematically.

The energy level scheme at $\nu \gg 1$ is shown in figure 1 (left-hand side) together with the spin projection states and the allowed transitions. Since iron borate is a canted antiferromagnet the magnetic fields at the two iron nuclei in the crystal unit cell are almost antiparallel. Now evaluations similar to those given above but for the coordinate system turned around the x axis by 180° (as shown in figure 1) have to be performed. In figure 1 (right-hand side) the level scheme for the second nucleus is displayed. The energy levels are the same as for the first nucleus but the states appropriate to the same levels correspond to the inverted spin projections.

The magnetic hyperfine field in $^{57}FeBO_3$ is a function of temperature. It drops down in approaching the transition to the paramagnetic state at the Néel temperature (in $^{57}FeBO_3$, $T_N \simeq 348$°K). So the positions of the energy levels change with temperature, following the parameter ν, eq. (2.13). In figure 2 the nuclear energy levels of the ground and excited states E_i^g and E_j^e are plotted as a function of the magnetic field when approaching T_N. The evolution of the hyperfine structure in this range is displayed in figure 3, where the transition energies, $E_{eg} = E_j^e - E_i^g$, between the ground and excited states are plotted. The hyperfine sextet structure collapses into a quadrupole doublet.

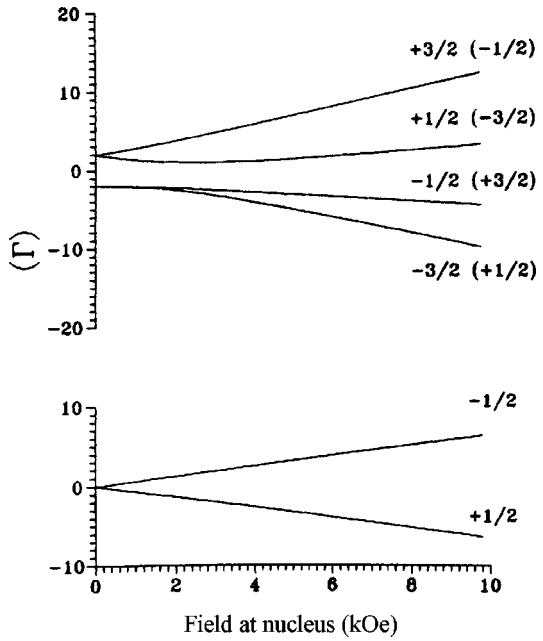

Figure 2. The nuclear energy levels of the ground and excited states plotted as functions of the magnetic hyperfine field when approaching the Néel temperature.

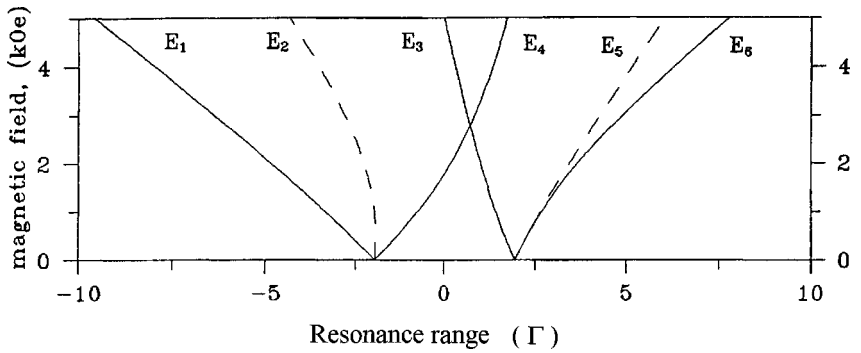

Figure 3. Evolution of the hyperfine structure of the $FeBO_3$ Mössbauer spectrum close to the Néel temperature. E_{ge} are the energies of the allowed transitions between the ground and excited states. The hyperfine sextet structure collapses into a quadrupole doublet consisting of the pair of lines $(1, 4)$ and the pair of lines $(3, 6)$.

The amplitudes of the spin projections in the excited nuclear state eq. (2.20) are depicted in figure 4 as functions of the hyperfine magnetic field near $T_{\rm N}$. These functions are given for the case where the quantization axis coincides with the axis of the magnetic hyperfine field, the z axis, while the main axis of the electric field gradient is perpendicular to it, in the direction of the x axis. To solve the scattering problem we now look at the nuclear susceptibility.

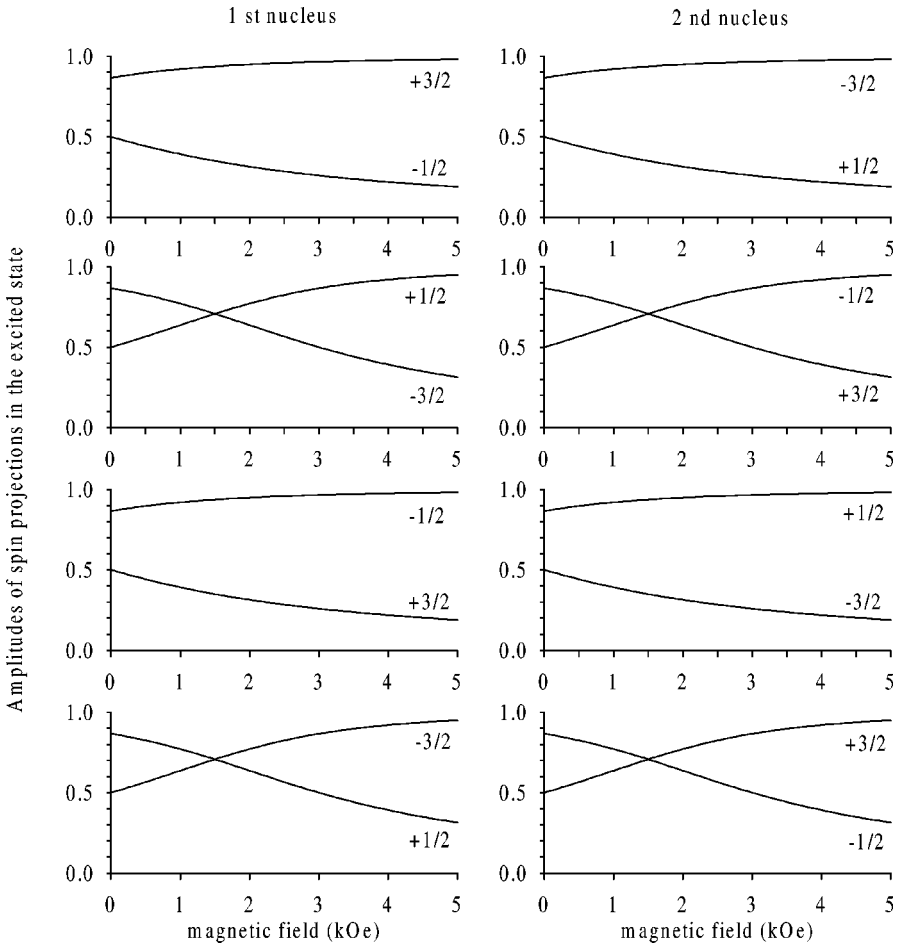

Figure 4. Amplitudes of the spin projections in the excited state of ^{57}Fe nuclei in the unit cell of $FeBO_3$ as functions of the magnetic hyperfine field close to the Néel temperature. The axis of quantization is taken parallel to the magnetic hyperfine field, i.e., the z axis, while the main axis of the electric field gradient is along the x axis.

2.2. Nuclear susceptibility matrix in pure nuclear Bragg scattering from iron borate

In optical theory the electric susceptibility associates the induced polarization of matter and the eigenwaves of the electromagnetic field in matter (see, e.g., [14]). The polarization of matter is understood as a sum of the induced electric moments per unit volume, both in electronic shells and in nuclei. Therefore the susceptibility contains nuclear and electronic contributions.

The susceptibility is closely related to the coherent scattering amplitude by the crystalline unit cell. To find the nuclear part of the susceptibility all possible scattering paths must be summarized, including scattering via all allowed nuclear transitions and all nuclei in the unit cell. A specific feature of our case is that the scattering via a single

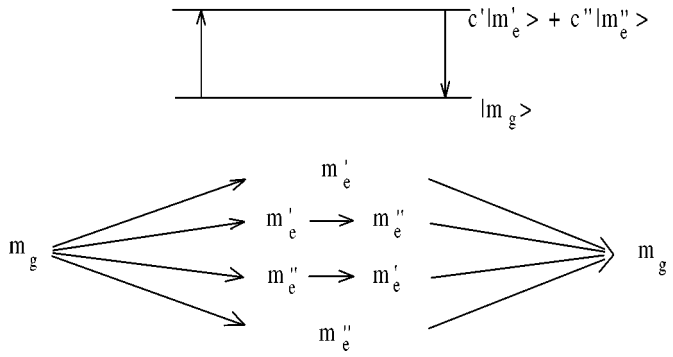

Figure 5. Scattering via a single nuclear transition at a separate nucleus shown schematically. It presents the interference of the four paths involving different spin projections in the excited state.

nuclear transition at a separate nucleus presents the interference of four paths, because the two spin projections are mixed at each excited level, see figure 5. For the case where a single diffracted wave is generated in an optically active medium the nuclear susceptibility turns out to be, in general, a (4×4) matrix with elements that present the probability amplitudes for the transitions between the two basic polarization states and the two allowed directions. The elements of the nuclear susceptibility matrix are (evaluated on the basis of [16])

$$\eta_{dd'}^{ss'}(E) = -\frac{3}{KV_0}\sigma_0\beta f_{\mathrm{LM}} \sum_{\mathrm{eg}} \frac{1}{v_{\mathrm{eg}} - i} \sum_a \mathrm{e}^{\mathrm{i}(\mathbf{k}_{d'} - \mathbf{k}_d)\mathbf{r}_a} \times \sum_{m'_{\mathrm{e}}, m''_{\mathrm{e}}} \left\langle \tfrac{1}{2}, m_{\mathrm{g}}; 1, q \middle| \tfrac{3}{2}, m'_{\mathrm{e}} \right\rangle \left\langle \tfrac{1}{2}, m_{\mathrm{g}}; 1, q' \middle| \tfrac{3}{2}, m''_{\mathrm{e}} \right\rangle c_{\mathrm{e},j}^{m'_{\mathrm{e}}} c_{\mathrm{e},j}^{m''_{\mathrm{e}}} \times (-1)^{q+q'} \left(\mathbf{h}_d^s \mathbf{u}_{-q}^a\right)\left(\mathbf{h}_{d'}^{s'} \mathbf{u}_{-q'}^a\right), \tag{2.21}$$

where:

- s, s' are indices of the basic σ and π polarization states,
- d, d' are indices of the scattering directions, each one takes the values $0, 1$; the relevant wave vectors $\mathbf{k}_d, \mathbf{k}_{d'}$ lie in the xz plane as shown schematically in figure 1,
- $K = 2\pi/\lambda$ is the radiation wave number,
- V_0 is the volume of the crystal unit cell,
- σ_0 is the resonance cross section,
- β is the resonance isotope abundance,
- f_{LM} is the recoilless scattering factor composed of the Lamb–Mössbauer factors in the d, d' directions:

$$f_{\mathrm{LM}} = \left[f(\mathbf{k}_d) f(\mathbf{k}_{d'})\right]^{1/2},$$

- $v_{\mathrm{eg}} = (E_{\mathrm{eg}} - E)/(\Gamma/2)$ is the deviation from the energy of the transition between the ground and excited state in units of the natural halfwidth of the nuclear level,

- $e^{i(\mathbf{k}_{d'}-\mathbf{k}_d)\mathbf{r}_a}$ is the scattering phase factor, where $\mathbf{r}_a$ is the coordinate of nucleus a in the unit cell,
- $\langle \frac{1}{2}, m_g; 1, q | \frac{3}{2}, m_e \rangle$ is the Clebsch–Gordan coefficient, where q is the magnetic quantum number of the radiation: $q = m_e - m_g$,
- $c_{e,j}^{m_e}$ is the amplitude of spin projection in the jth sublevel of the excited state,
- $\mathbf{h}_d^s$ is the magnetic polarization vector of incident or scattered radiation wave, vectors $\mathbf{h}_{0,1}^{\sigma}$ lie in the scattering plane, while vectors $\mathbf{h}_{0,1}^{\pi}$ are perpendicular to it, and
- $\mathbf{u}_{-q}^a$ are the spherical unit vectors in the coordinate systems at the ath nucleus in the unit cell: $\mathbf{u}_0 = \mathbf{u}_z$ – the unit vector in the direction of the quantization axis (the direction of the local magnetic field at the nucleus in our case), $\mathbf{u}_{\pm 1} = \mp(\mathbf{u}_x \pm \mathbf{u}_y)/\sqrt{2}$. Since the local fields in the unit cell are antiparallel we have to deal with the two different coordinate systems at the nuclei for the description of nuclear transitions (see figure 1). We shall call

$$P_{dd'qq'}^{ss'} = (-1)^{q+q'} \left(\mathbf{h}_d^s \mathbf{u}_{-q}\right) \left(\mathbf{h}_{d'}^{s'} \mathbf{u}_{-q'}\right)$$

the polarization factor.

The inner sum in eq. (2.21) presents the summation over the four paths depicted in figure 5, the next two are summations over the nuclei in the unit cell and the allowed nuclear transitions. Since the white X-ray SR is able to excite at once all nuclear transitions we deal with a quite complicated case of interference where $4 \times 2 \times 6 = 48$ terms contribute to build up each element of the susceptibility matrix. The polarizations, amplitudes and phases of the interfering contributions are determined by the structural and polarization factors, by Clebsch–Gordan coefficients and by the amplitudes of spin projection states. Keep in mind that we have chosen the electronically (or structurally) forbidden reflections where the scattering phase factors have opposite signs.

We distinguish the two groups of interfering contributions within and in-between the nuclear transitions. So we shall speak of intra- and inter-resonance interference. When regarding the whole unit cell (two nuclei) and only the Bragg scattering direction the intra-resonance interference leads to a quite different behavior of the susceptibility at different transitions. Because of the change of sign of the phase factor all contributions to the susceptibility belonging to $q = 0$ (in particular, the lines 2 and 5 in the ^{57}Fe Mössbauer spectrum) disappear due to the intra-resonance destructive interference. The contributions with $q = \pm 1$ (lines 1, 3, 4, 6) survive because the change of sign of the phase factor is compensated by the change of sign of the polarization factor. However, the lines 1, 3, 4, 6 exhibit quite a different behavior in the range where the magnetic and the quadrupole interactions are comparable (in the vicinity of T_N), see figure 6. Only lines 3 and 6 do not suffer from intra-resonance interference while lines 1 and 4 vanish. It is of interest that on the way to zero magnetic field the strength of line 3 drops to zero first and then grows again.

The inter-resonance interference becomes effective when the transition energies come close to each other. This interference destroys the contributions within the

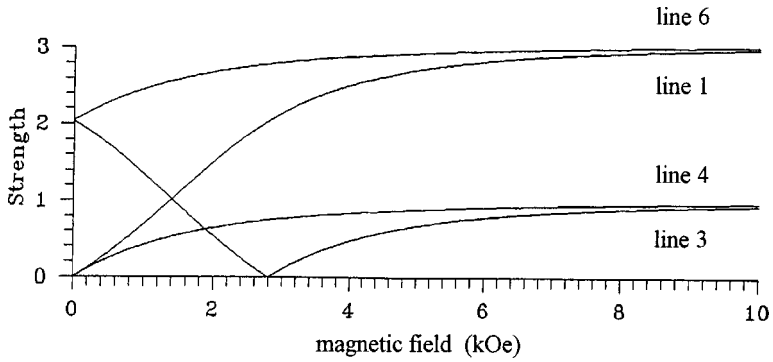

Figure 6. Effect of intra-resonance interference on the strength of the hyperfine components in the Mössbauer diffraction spectrum of $FeBO_3$ (reflection (3 3 3)) when approaching the Néel temperature. The inter-resonance interference is not accounted for in the simulation.

groups of the 1, 4 lines and 3, 6 lines which get together, so that above the Néel temperature the elements of nuclear susceptibility η_{01} and η_{10} become zero and the coherent scattering vanishes.

As seen from figure 3, it is just the pair of the 1, 4 and that of the 3, 6 transitions which form the quadrupole doublet near $T_{\rm N}$. It occurs that the combined destructive intra- and inter-resonance interference destroys the left-hand line of the doublet much faster than the right-hand one. For this reason a little below $T_{\rm N}$ the susceptibility has a pseudo single line resonance structure which provides a basis for performing a single line synchrotron Mössbauer source.

2.3. Mössbauer diffraction spectrum of iron borate at $T_{\rm N}$

Making use of eq. (2.21) one can see that the nuclear susceptibility for polarized incident radiation with a basic σ or π polarization state reduces to a matrix of second rank, e.g., for σ polarization

$$\eta_{dd'}^{ss'} = \begin{vmatrix} \eta_{00}^{\sigma\sigma} & \eta_{01}^{\sigma\pi} \\ \eta_{10}^{\pi\sigma} & \eta_{11}^{\pi\pi} \end{vmatrix}. \tag{2.22}$$

Thus the incident waves, with the basic polarization states, are not mixed in pure nuclear diffraction due to antiferromagnetic order. As seen from eq. (2.22) the polarization plane rotates by $\pi/2$ due to diffraction.

The electronic susceptibility χ is evaluated in a standard way, see, e.g., [16]. In the case under study its matrix elements $\chi_{01}^{\sigma\pi} = \chi_{10}^{\sigma\pi} = 0$, due to the choice of the structurally forbidden reflections. The other two are constant, for instance, for the Bragg reflections from $FeBO_3$ $(n\,n\,n)$ they are $\chi_{00}^{\sigma\sigma} = \chi_{11}^{\pi\pi} = (8.16 + {\rm i}0.183) \times 10^{-6}$.

The set of dynamical wave equations (in our case two) together with the boundary conditions for the symmetric Bragg reflections $(n\,n\,n)$ is used to find the propagation

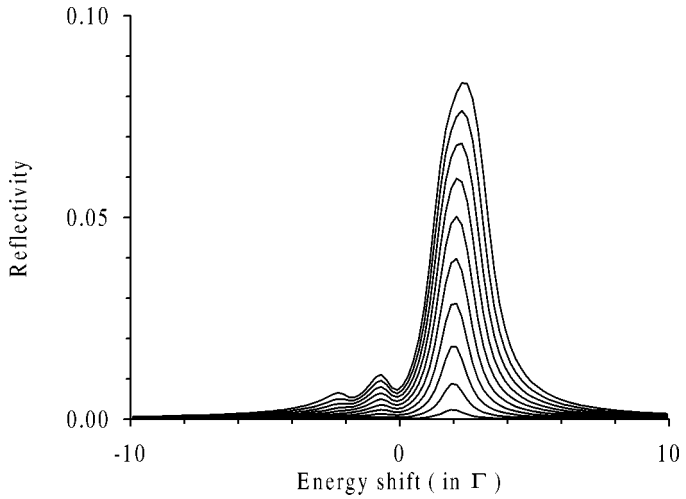

Figure 7. Energy dependence of the reflectivity of $FeBO_3$ (reflection (3 3 3)) integrated in the range $\Theta_B \pm 2$ arcsec at different values of the magnetic hyperfine field. The shapes of the curves are the expected energy distributions of the Mössbauer radiation reflected by the iron nuclei in $^{57}FeBO_3$ after excitation with SR.

vectors inside the crystal, the polarization states and the scalar amplitudes of the constituent eigenwaves. In the case of a thick crystal (of effective thickness $T = \eta_{00} K d \gg 1$, where η_{00} is taken at $E = E_{eg}$) the solution for the reflectivity is found (on the basis of [16,17]) to be

$$R = \frac{|\tilde{\eta}_{10}^{\pi\sigma}|^2}{|2\varepsilon^{(1)} - \tilde{\eta}_{00}^{\sigma\sigma}|^2} \tag{2.23}$$

with

$$\varepsilon^{(1)} = \tfrac{1}{4}\Big\{\tilde{\eta}_{00}^{\sigma\sigma} - \tilde{\eta}_{11}^{\pi\pi} + \alpha - \sqrt{\left(\tilde{\eta}_{00}^{\sigma\sigma} + \tilde{\eta}_{11}^{\pi\pi} - \alpha\right)^2 - 4\tilde{\eta}_{01}^{\sigma\pi}\tilde{\eta}_{10}^{\pi\sigma}}\Big\},$$

where the angular parameter $\alpha = -2\Delta\vartheta \sin 2\Theta_B$ and $\Delta\vartheta$ is the angular deviation from the Bragg angle Θ_B, $\tilde{\eta}_{dd'}^{ss'}$ is the sum of the nuclear and electronic susceptibilities, defined above. The reflectivity integrated in the range $\Theta_B \pm 2$ arcsec at different values of the local magnetic field is shown in figure 7. The shape of the curves characterizes the expected energy distributions of the Mössbauer radiation generated by the nuclear array in $^{57}FeBO_3$ excited by SR. Along with the dominant single line the weak lines at the left-hand side are seen which bear some traces of the quadrupole doublet. Such a distribution of the source radiation can easily be accounted for as an instrumental function in fitting the experimental data with the theory.

3. Experimental studies

3.1. Nuclear reflectivity of iron borate measured with a Mössbauer source

The energy dependence of the reflectivity of the iron borate single crystal was tested first with a conventional Mössbauer source. The unpolarized source radiation was incident on a single-crystal platelet of iron borate (the planes $(n\,n\,n)$ are parallel to the crystal surface) set for the *electronically forbidden* Bragg reflection. The crystal was mounted in an oven where it could be heated up to the Néel temperature. An external magnetic field of about 10 mT was applied along the crystal to magnetize it perpendicular to the scattering plane (xz-plane in figure 1). The hyperfine magnetic fields were almost normal to the external field (as they should be in a canted antiferromagnet) and lie along the z axis. The application of an external field allowed us to extend the magnetic transition range beyond T_{N} and essentially to slow down the decrease of the hyperfine field [18]. In figure 8 the Mössbauer diffraction spectra from the crystal planes (3 3 3) are displayed at different temperatures in the range from room

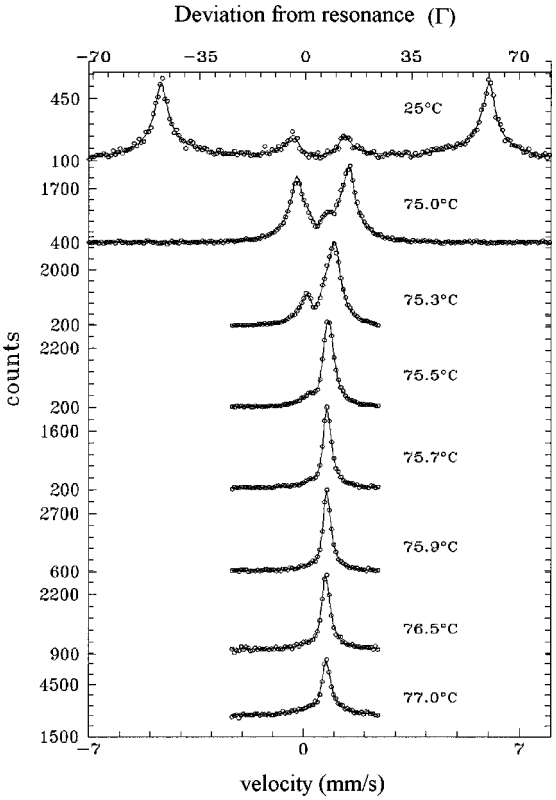

Figure 8. Mössbauer diffraction spectra of resonant γ radiation (^{57}Co(Cr) source) from a $^{57}FeBO_3$ crystal at different temperatures. The solid lines are fits using the angle integrated reflectivity function eq. (2.23) (the fits were accomplished by M.V. Gusev [13]).

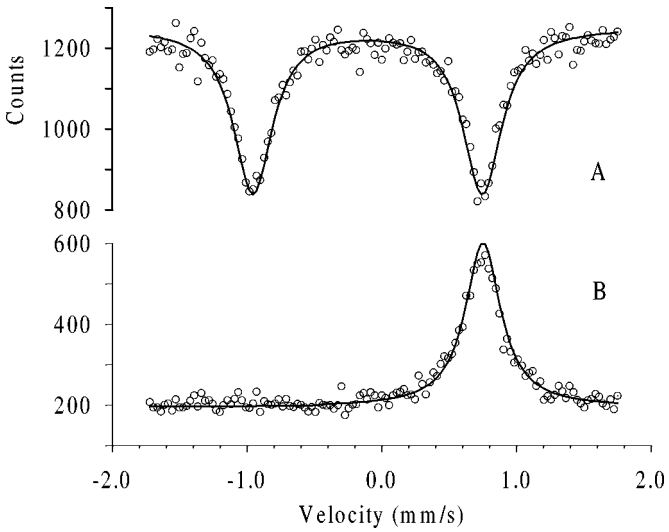

Figure 9. (A) Mössbauer absorption spectrum of resonant γ radiation of a ^{57}Co(Cr) source by a thin standard absorber of sodium nitroprusside. The solid line is a fit with the transmission integral. (B) Mössbauer diffraction spectrum of the same radiation by a $^{57}FeBO_3$ crystal at the Néel temperature ((3 3 3) Bragg reflection). A magnetic field of 10 mT was applied along the crystal surface perpendicular to the scattering plane. The solid line is a fit with a Lorentzian line.

temperature up to the Néel temperature. The four resonance lines corresponding to $q = \pm 1$ are present in the spectrum taken at room temperature, which are only allowed in the case of pure nuclear diffraction (see section 2). It is clear that the hyperfine structure collapses with increasing temperature and a single line spectrum forms (we recall that it exists in the presence of magnetic splitting only). The Mössbauer diffraction spectrum measured near T_N (spectrum B) is displayed in figure 9 in comparison with a Mössbauer absorption spectrum in a thin standard absorber of sodium nitroprusside (spectrum A). The width Γ_s of the Mössbauer source line was determined from the fit of the spectrum (A): $\Gamma_s = 2.0\Gamma_0$. Using this width the spectrum (B) was fitted with a Lorentzian line of width $1.3\Gamma_0$. This value characterizes the energy width of the nuclear reflection from the crystal of a noncollimated incident beam. Another important characteristic provided by this measurement is the energy position of the resonance reflection. Figure 8 shows that it coincides very well with one of the resonances in sodium nitroprusside. It was expected that the crystal of iron borate placed in a white SR beam under the conditions just described will radiate Mössbauer radiation in the Bragg direction within the narrow band reflection.

3.2. Synchrotron Mössbauer radiation

3.2.1. Scheme of the synchrotron Mössbauer source

The scheme for generation of ^{57}Fe Mössbauer radiation at a SR facility is displayed in figure 10. The experiment was performed at the Nuclear Resonance Beam-

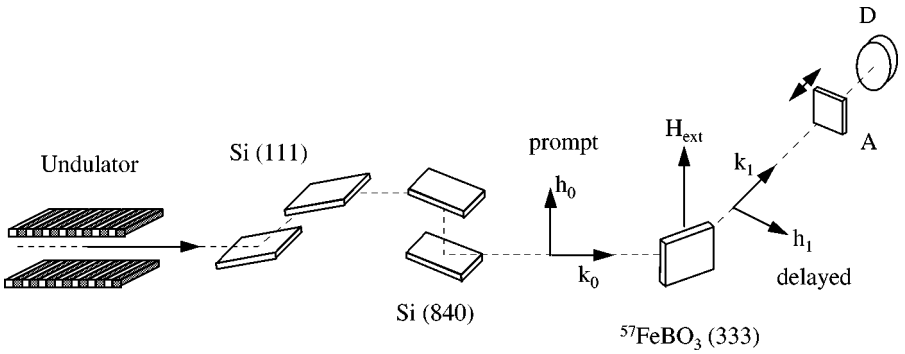

Figure 10. Scheme of the experimental setup for the generation of ^{57}Fe Mössbauer radiation at the ESRF facility. Monochromatization and polarization of the SR were provided by a double-crystal Si(1 1 1) monochromator and a channel-cut Si(8 4 0) polarizer, respectively. The pure nuclear Bragg reflection was the (3 3 3) reflection of a $^{57}FeBO_3$ single crystal put in an oven. The absorber (A), driven by a Mössbauer transducer, and the APD detector (D) are mounted along the diffracted beam.

line [19] of the European Synchrotron Radiation Facility (ESRF). SR is naturally σ-polarized (the electric vector lies in the orbital plane of the electrons, horizontal in the figure) up to 99%. The undulator of the beam line was tuned to provide 14.413 keV radiation. A Si(1 1 1) double crystal monochromator reduced the bandwidth to 2.8 eV at the nuclear resonance energy. An asymmetric Si(8 4 0) Bragg double reflection was used for further monochromatization and polarization of the beam. This particular reflection has a scattering angle of $2\Theta_B = 90.2^\circ$ for 14.4 keV radiation. The (8 4 0) reflection reduced the content of the π-polarized component of the radiation from a level of 1% to less than 10^{-4}% and the radiation bandwidth to $\sim$400 meV (instead of the Si(8 4 0) monochromator a high resolution type can also be used, see, e.g., [19], which reduces the bandwidth to $\sim$1–4 meV). The scattering in the system of Si monochromators takes place in the vertical plane. The outgoing beam was highly directed, its divergence was about 2×7 arcsec and its cross section was 0.5×2.0 mm^2. The flux after the (8 4 0) reflection was about 300 cps per natural linewidth Γ_0 at 130 mA electron current in the storage ring.

The pulsed X-ray beam was incident on a single-crystal of iron borate set for the *electronically forbidden* Bragg reflection (3 3 3) in a horizontal plane. The crystal was placed in the conditions described in the previous section. As was said earlier, the nuclear diffraction in iron borate rotates the polarization plane by 90°, turning the magnetic polarization vector into the horizontal plane.

A careful adjustment of the crystal with respect to the incident SR beam was undertaken to avoid so-called Umweg reflections which could contribute to the electronic reflectivity. Setting the crystal as far as possible off all Umweg reflections allowed us to obtain a suppression of the electronic reflectivity to a level of $\sim 10^{-10}$ [20]. Such a high suppression of the nonresonant component of SR permitted detection of the scattered radiation *without any time gating*, as illustrated in figure 10, where the time dependence of the (3 3 3) reflection is shown for a fully open time window (a

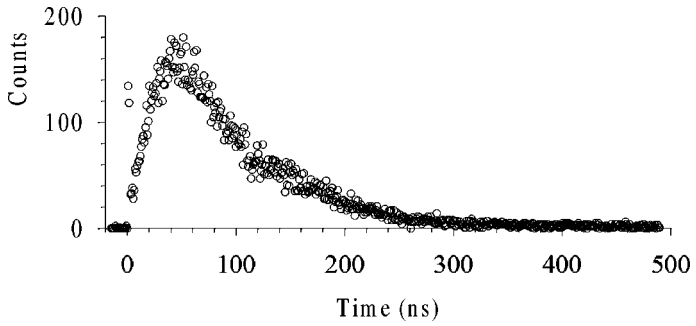

Figure 11. Time distribution of Bragg reflected radiation from a $^{57}FeBO_3$ single crystal (reflection (3 3 3)). The first two channels represent prompt electronic scattering. All remaining channels represent delayed nuclear emission. The contribution of prompt radiation is about 1% of the total reflected intensity.

fast avalanche photodiode counter was used [21]). The time spectrum contains only a small part of the prompt radiation (see the first two channels) in contrast to the intensive extended spectrum part of delayed radiation. The prompt and delayed parts are related to electronic and nuclear scattering, respectively. In the figure the contribution of the prompt radiation is about 1% of the total reflected intensity. Therefore, almost all radiation is that re-emitted by nuclei in iron borate. It is fully recoilless radiation due to elastic coherent scattering. Thus the crystal can be considered as a *source of pure spatially coherent Mössbauer radiation*. This synchrotron Mössbauer source can be used for performing a Mössbauer measurement in the conventional energy scheme.

In order to achieve optimal conditions several temperatures near T_N should be tested for choosing the optimum regime of the SM source. The intensity of the source radiation and its energy distribution will follow the functions displayed in figure 7. One has to find a compromise between the intensity and the line width. In the experiments performed until now at ESRF the reflected intensity was in the range of 100–700 cps with linewidth $2.5 \div 3.5\Gamma_0$.

3.2.2. Mössbauer spectra taken with the SM source

The properties of the SM source were illustrated in several measurements with the use of widely spread nuclear resonant absorbers. The results are presented in figures 12–14. An absorber was placed on the reflected beam, see figure 10, and driven by a conventional Mössbauer transducer.

The Mössbauer spectra of stainless steel (SS) foils of 1 and 10 μm thickness (enriched to 95% in ^{57}Fe) are shown in figure 12. Single-line spectra with a resonance effect of $\varepsilon = 70$ and 86% ($\varepsilon = 100\% \cdot (I_\infty - I_r)/I_\infty$) were observed, yielding a linewidth of the source radiation equal to $2.9\Gamma_0$ and a Lamb–Mössbauer factor of the source equal to unity.

In order to check the degree of polarization of the SM radiation, Mössbauer spectra of a 1 μm thick iron foil (95% ^{57}Fe) were measured, see figure 13. The upper spectrum was taken with a nonmagnetized foil. The characteristic 6-line pattern was obtained in this case. The ratio of the line intensities reveals the presence of

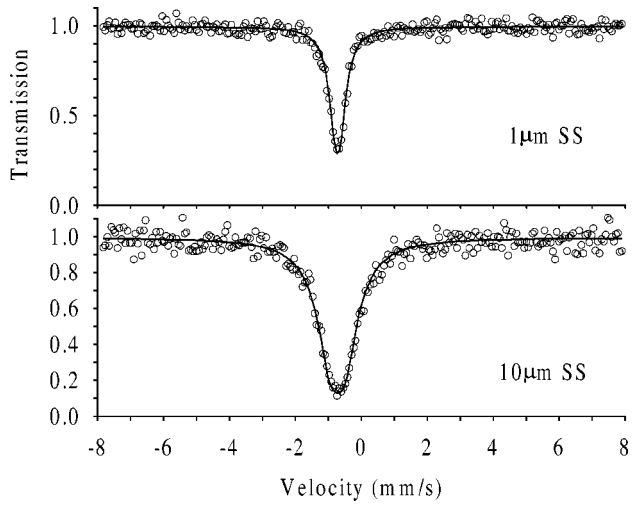

Figure 12. Mössbauer transmission spectra of 1 μm and 10 μm thick stainless steel foils (95% ^{57}Fe) measured with radiation from the SM source. The solid curves are fits with Lorentzian lines. The fit yields a linewidth of the source radiation of $2.9\Gamma_0$ and a Lamb–Mössbauer factor of unity.

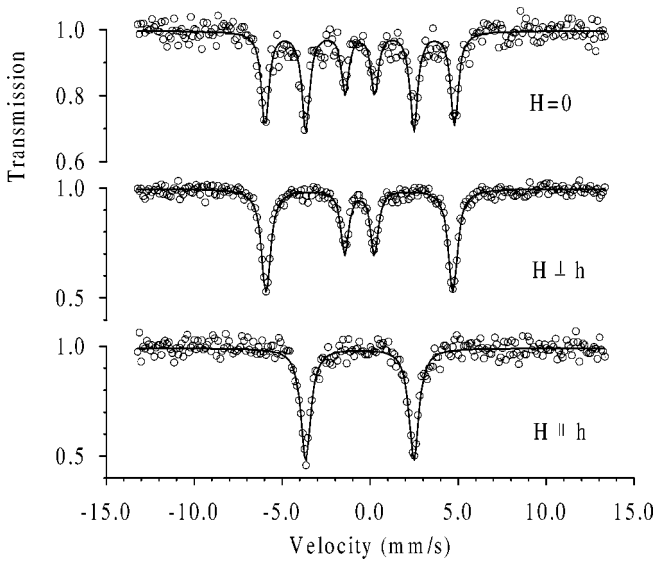

Figure 13. Mössbauer transmission spectra of an ^{57}Fe foil of 1.3 μm thickness measured with the SM source at different magnetic fields. The solid lines are fits using the transmission integral with 100% linearly polarized and recoilless radiation.

off-plane magnetization. The other two spectra were measured when the foil was magnetized in an external magnetic field of 60 mT in the vertical and horizontal planes. Within statistics, only the four or two resonances related to the nuclear $q = \pm 1$ and $q = 0$ transitions, respectively, were observed. This result gives clear evidence of the

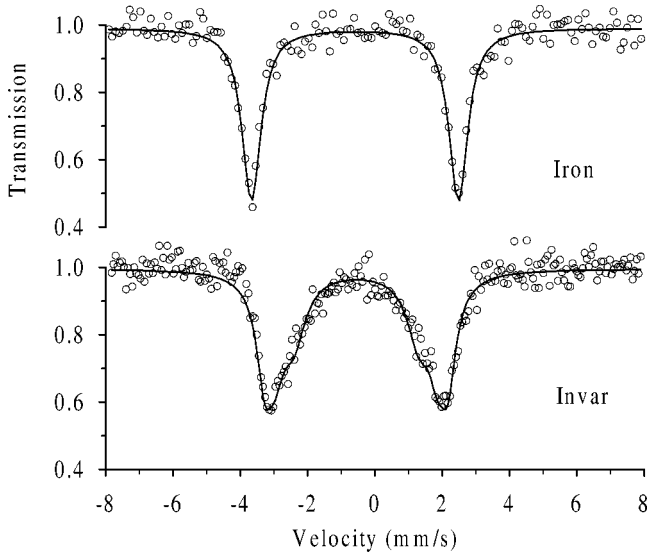

Figure 14. Mössbauer transmission spectra of thin foils of iron metal and invar alloy measured with the SM source. Both the iron foil of 1.3 μm thickness and the invar foil of 1 μm thickness were magnetized: $\mathbf{B}_{\rm ext} \,||\, \mathbf{h}_1$. The solid lines are fits using the transmission integral. The field strength distribution is simulated by three Lorentzians.

polarization state of the source radiation: the radiation is of pure linear polarization with the magnetic vector in the horizontal plane. A comparably high polarization of radiation from a conventional Mössbauer source has been obtained recently in [22].

The advantage of the pure polarization state of SM radiation was demonstrated by measuring a Mössbauer spectrum of an invar alloy ($Fe_{65}Ni_{35}$). The possibility to selectively excite the nuclear resonances essentially simplifies the observation of anomalies in their shapes. In figure 14 the Mössbauer spectrum of a 1 μm thick invar foil (95% ^{57}Fe) magnetized along the magnetic polarization vector is shown and compared with the analogous spectrum of a 1 μm thick iron foil. The asymmetric distribution of the hyperfine magnetic field strength characteristic for the invar alloy is directly seen from the data.

4. Summary and prospects

Coherent Mössbauer radiation from ^{57}Fe nuclei can be produced at an SR facility. The radiation is generated in pure nuclear diffraction of SR from a single crystal of iron borate slightly below the Néel temperature. The coherent scattering is noticeable there for its strong *intra-resonance interference* because of mixing the spin projections in the excited state and for its intensive *inter-resonance interference* due to the collapse of the hyperfine structure. The combined interference process results in a *single-line profile of the nuclear reflectivity* within $\sim 1 \div 3$ nuclear level widths. The elastic character of scattering provides *fully recoilless radiation. High directionality and polarization*

of the radiation are defined both by the undulator–monochromator system and by a high structural and magnetic perfection of the nuclear system. Making use of a structurally forbidden reflection in such a crystal leads to an *extremely high suppression of the electronic scattering, by a factor of about* 10^{-10}. This allows one to perform time integrated Mössbauer measurements. From this the great practical advantage of the SM source follows, namely the possibility to exploit it at any storage ring mode.

In a conventional Mössbauer experiment it is convenient to have the source Doppler shifted rather than the sample. Such a modification of the present SM source can be made, for instance, by using an especially light oven and a driving unit which supplies a precise translation motion, the solution in [23], or by employing an intermediate nonresonant Bragg reflector [24,25]. Some improvements of the SM source characteristics, namely of its power and linewidth, are possible by choosing optimal diffraction conditions.

The special properties of the SM source open good perspectives for its application both in transmission and scattering Mössbauer experiments. First of all one should note that when necessary, complementary studies of nuclear resonance in energy and time domains are possible. The high degree of polarization can be employed for studying different kinds of static distributions of magnetic moments in materials. Recently the investigation of moment canting in the $Fe_{78}Si_9B_{13}$ amorphous alloy was accomplished with the use of a SM source [26]. It also gives the possibility to selectively excite a part of the nuclear target or a subsystem characterized by a particular hyperfine environment and to study the hyperfine interaction in this part. The possibility of energy selective excitation in combination with resonance purity, directionality and polarization of the SM source radiation offers a beneficial application for measuring the autocorrelation function of ^{57}Fe atoms as a function of their chemical environment, e.g., in the situation described in [27].

The ideal resonance purity of the source radiation (100% recoil-free) allows one to measure directly the Lamb–Mössbauer factor of the sample of interest. The directionality of the source radiation provides the possibility to investigate anisotropic diffusion, e.g., jump diffusion in single crystals. One should mention the possibility to apply the RSMR (Rayleigh Scattering of Mössbauer Radiation) technique at a much higher intensity for studying quasi-elastic scattering from single crystals.

Another group of experiments could benefit from the very small beam cross section, which allows the use of small samples as required, e.g., for high-pressure cells or the investigation of small parts of a sample in the case of sample or temperature inhomogeneities.

Special applications are opened in the field of nuclear resonant dynamical diffraction of γ-radiaton, where the extreme brilliance of the new source is of greatest importance (to get a similar flux of recoil-free γ-radiation into a solid angle of 10×35 μrad^2 would require a radioactive Mössbauer source of about 1000 Ci of ^{57}Co). A review of the phenomena in this field can be found for instance in [28]. For diffraction studies it is of interest that the SM source has an extremely low divergence in the plane per-

pendicular to the beam, thus allowing for instance the study of noncoplanar n-beam multiple resonant diffraction [29]. It also allows the studies of different combinations of Borrmann and Kagan–Afanas'ev effects in searching for the possibility to control the interaction of γ-radiation with electronic and nuclear subsystems of matter. These studies are essential in connection with the problem of γ-ray lasing [30].

Acknowledgements

The author is grateful to Dr. S.L. Popov, Dr. W. Potzel and Dr. U. van Bürck for a critical reading of the manuscript and valuable comments. Support of this work was partially provided by INTAS-RFBR under Contract No. 95-0586.

References

[1] S. Ruby, J. Phys. (Paris) Colloq. 35 (1974) C6-209.
[2] Yu. Kagan, A.M. Afanas'ev and V.G. Kohn, J. Phys. C 12 (1979) 615.
[3] G.T. Trammel and J.P. Hannon, Phys. Rev. B 18 (1978) 165; 19 (1979) 3835.
[4] E. Gerdau and U. van Bürck, in: *Resonant Anomalous X-ray Scattering*, eds. G. Materlik, C.J. Sparks and K. Fischer (Elsvevier, Amsterdam, 1994) p. 589.
[5] G.V. Smirnov, Hyp. Interact. 97/98 (1996) 551; in: *X-ray and Inner-Shell Processes*, AIP 389 (1997) 323.
[6] G.V. Smirnov, M.V. Zelepukhin and U. van Bürck, Pis'ma Zh. Eksper. Teoret. Fiz. 43 (1986) 274 (JETP Lett. 43 (1986) 352).
[7] A.I. Chumakov, M.V. Zelepukhin, G.V. Smirnov, U. van Bürck, R. Rüffer, R. Hollatz, H.D. Rüter and E. Gerdau, Phys. Rev. B 41 (1990) 9545.
[8] E. Matthias, W. Schneider and R. Steffen, Phys. Rev. 125 (1962) 261.
[9] E. Mathias, W. Schneider and R. Steffen, Ark. Fys. 24 (1963) 97.
[10] W. Kündig, Nucl. Instrum. Methods 48 (1967) 219.
[11] G.R. Hoy and S. Chandra, J. Chem. Phys. 47 (1967) 961.
[12] M.V. Zelepukhin, Ph.D. thesis, Kurchatov Insitute, Moscow (1990).
[13] M.V. Gusev, Diploma thesis, Kurchatov Institute, Moscow (1992);
M.V. Gusev, G.V. Smirnov, M.V. Zelepukhin and U. van Bürck, in: *ICAME '93*, Vancouver (1993) 46 5-17B.
[14] G.V. Smirnov, this issue, section II-2.
[15] M.E. Rose, *Elementary Theory of Angular Momentum* (Wiley, New York, 1957).
[16] Yu. Kagan and A.M. Afanas'ev, Z. Naturforsch. 28a (1973) 1351.
[17] Yu. Kagan, A.M. Afanas'ev and I.P. Perstnev, Zh. Eksper. Teoret. Fiz. 54 (1986) 1530; JETP 27 (1968) 819.
[18] M.V. Zelepukhin, G.V. Smirnov and U. van Bürck, Questions of Atomic Science and Technique, Series: General and Nuclear Physics 4(33) (1985) 76.
[19] R. Rüffer and A.I. Chumakov, Hyp. Interact. 97/98 (1996) 589; this issue, section I-1.
[20] G.V. Smirnov, U. van Bürck, A.I. Chumakov, A.Q.R. Baron and R. Rüffer, Phys. Rev. B 55 (1997) 5811.
[21] A.Q.R. Baron, R. Rüffer and J. Metge, Nucl. Instrum. Methods A 400 (1997) 124.
[22] J. Jäschke et al., to be published.
[23] S. Kikuta, Y. Yoda, Y. Kudo, K. Izumi, T. Ishikawa, C. Suzuki, H. Ohno, H. Takei, K. Nakayama, X. Zhang, T. Matsushita, S. Kishimoto and M. Ando, Japan J. Appl. Phys. 30 (1991) L1686.

[24] A. Nielsen and J. Olsen, Nucl. Instrum. Methods 52 (1967) 173.
[25] G. Schupp, K. Barnes, W.B. Yelon and J.G. Mullen, Hyp. Interact. 92 (1994) 1149.
[26] Q.A. Pankhurst, N.S. Cohen, L. Fernández Barquín and G.V. Smirnov, ESRF Report HE-182 (1998).
[27] T.A. Stephens and B. Fultz, Phys. Rev. Lett. 78 (1997) 366.
[28] G.V. Smirnov and A.I. Chumakov, in: *Resonant Anomalous X-ray Scattering*, eds. G. Materlik, C.J. Sparks and K. Fischer (Elsevier, Amsterdam, 1994) p. 609.
[29] V.G. Kohn, Zh. Eksper. Teoret. Fiz. 105 (1994) 665 (JETP 78 (1994) 357).
[30] G.C. Baldwin and J.C. Solem, Rev. Modern Phys. 69 (1997) 1085.